The Astrophysical Journal, 744:169 (4pp), 2012 January 10 doi:10.1088/0004-637X/744/2/169

143 GHz BRIGHTNESS MEASUREMENTS OF URANUS, NEPTUNE, AND OTHER SECONDARY CALIBRATORS WITH BOLOCAM BETWEEN 2003 AND 2010

J. Sayers, N. G. Czakon, and S. R. Golwala
Department of Physics, Mathematics, and Astronomy, California Institute of Technology, Pasadena, CA 91125, USA; jack@caltech.edu
Received 2011 October 16; accepted 2011 November 30; published 2011 December 22

ABSTRACT

Bolocam began collecting science data in 2003 as the long-wavelength imaging camera at the Caltech Submillimeter Observatory. The planets, along with a handful of secondary calibrators, have been used to determine the flux calibration for all of the data collected with Bolocam. Uranus and Neptune stand out as the only two planets that are bright enough to be seen with high signal-to-noise in short integrations without saturating the standard Bolocam readout electronics. By analyzing all of the 143 GHz observations made with Bolocam between 2003 and 2010, we find that the brightness ratio of Uranus to Neptune is 1.027 ± 0.006, with no evidence for any variations over that period. Including previously published results at $\simeq$150 GHz, we find a brightness ratio of 1.029 ± 0.006 with no evidence for time variability over the period 1983–2010. Additionally, we find no evidence for time variability in the brightness ratio of either Uranus or Neptune to the ultracompact H II region G34.3 or the protostellar source NGC 2071IR. Using recently published *Wilkinson Microwave Anisotropy Probe* results we constrain the absolute 143 GHz brightness of both Uranus and Neptune to $\simeq$3%. Finally, we present $\simeq$3% absolute 143 GHz peak flux density values for the ultracompact H II regions G34.3 and K3-50A and the protostellar source NGC 2071IR.

Key words: instrumentation: photometers – ISM: individual objects (G34.3, K3-50A, NGC 2071IR) – planets and satellites: individual (Neptune, Uranus)

Online-only material: color figures

1. INTRODUCTION

The past two decades have seen vast improvements in the sensitivity and detector counts of broadband (sub)millimeter imaging cameras, from single pixel receivers to background-limited kilopixel arrays (e.g., Duncan et al. 1990; Holland et al. 1999, 2006; Runyan et al. 2003; Dowell et al. 2003; Haig et al. 2004; Carlstrom et al. 2011; Swetz et al. 2011). Many of these instruments have relied on the planets, along with a handful of secondary calibrators, to obtain $\lesssim$10% flux calibrations (e.g., Hill et al. 2009; Rudy et al. 1987; Griffin & Orton 1993, hereafter G93; Sandell 1994). Alternatively, some of the large-scale survey instruments have used cosmic microwave background (CMB) measurements to calibrate their data to even better precision (e.g., Reichardt et al. 2009). However, calibrating from the CMB is only practical for instruments that image $\gtrsim$100 deg^2, and therefore cannot be done in many cases. When planets and secondary calibrators are used, the accuracy of the flux calibration is often limited by uncertainties in the brightness of these calibrators rather than by measurement uncertainties (e.g., Sayers et al. 2009). Consequently, accurate measurements of the absolute brightness of the planets and secondary calibrators, along with a detailed understanding of any temporal variability in these brightnesses, are critical to maximizing the scientific potential of current and future (sub)millimeter cameras.

Until recently, systematic uncertainties in the brightness of Uranus and Neptune have been $\simeq$5%–10%, owing to uncertainties in the Martian brightness used to determine the absolute brightness of each of these planets (Wright 1976; Rudy et al. 1987; Orton et al. 1986, hereafter O86; G93). However, recently published *Wilkinson Microwave Anisotropy Probe* (*WMAP*) results have significantly improved the constraints on the brightness of Mars ($\simeq$1%) and Uranus ($\simeq$3%) by calibrating them relative to the CMB (Page et al. 2003; Hill et al. 2009; Weiland et al. 2011). *WMAP* has also published CMB-calibrated brightness measurements of Neptune accurate to 8% (Weiland et al. 2011).

Additionally, recently published results have shown evidence for an $\simeq$10% decrease in the brightness of Uranus at 8.6 and 90 GHz over the $\simeq$20 year period from the mid-1980s to the mid-2000s (Klein & Hofstadter 2006, hereafter Kl06; Kramer et al. 2008, hereafter Kr08), which have been attributed to changes in the relative viewing angle of the planet from Earth due to its large obliquity of 82 deg. Note that over the period of observations in Kl06 and Kr08 the sub-Earth point (SEP) latitude of Uranus ranged from a minimum of -82 deg in 1985 to a maximum of -7 deg in 2005. These data indicate that the brightness of Uranus increases as the magnitude of the SEP latitude increases (i.e., the south pole of Uranus is brighter than the equatorial regions). Further evidence for this scenario comes from resolved centimeter-wave images of Uranus, which indicate that the poles are brighter than the equatorial regions (Orton et al. 2007).

2. OBSERVATIONS

Bolocam is a large-format bolometric camera with an 8 arcmin field of view capable of observing at either 143 or 268 GHz. Bolocam began collecting scientific data in early 2003 at the Caltech Submillimeter Observatory (CSO) and was commissioned as a facility instrument later that year (Haig et al. 2004). In this paper we focus exclusively on 143 GHz Bolocam data, which were collected between 2003 and 2010 during nine separate observing runs (see Table 1). All of the data collected with Bolocam have been calibrated using the planets (generally Uranus and Neptune), along with sources given in Sandell (1994). The Bolocam flux calibration procedure is described in detail in Laurent et al. (2005) and Sayers et al. (2009), and we briefly describe the details below.

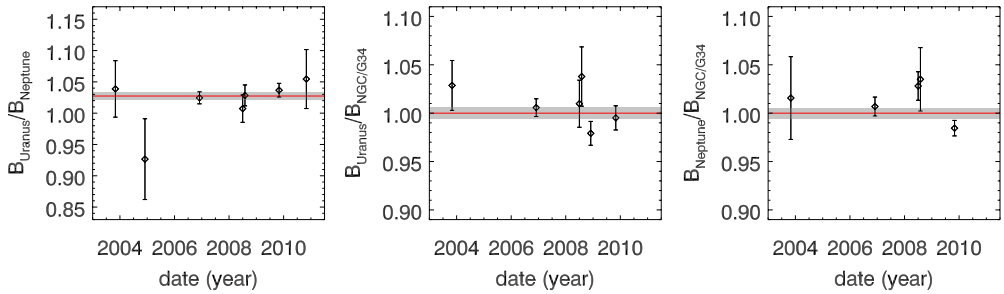

Figure 1. From left to right, Bolocam measurements of the brightness ratio of Uranus to Neptune, the relative brightness ratio of Uranus to NGC 2071IR or G34.3, and the relative brightness ratio of Neptune to NGC 2071IR or G34.3 for the period from 2003 to 2010. The red line shows the best-fit mean value of the brightness ratio (equal to 1 by definition for the center and right plots), and the gray band represents the 1σ confidence region. Our data show no evidence for temporal variations in any of these brightness ratios.

(A color version of this figure is available in the online journal.)

Table 1
Summary of 143 GHz Bolocam Observations

Date	Uranus	Neptune	NGC 2071IR	G34.3	K3-50A
2003 Nov	6	5	9	0	0
2004 Nov	11	20	0	0	0
2006 Nov	6	3	15	0	0
2008 June	2	3	0	5	0
2008 July	1	2	0	10	2
2008 Nov	7	0	8	0	0
2009 Oct	5	21	9	0	0
2010 Feb	0	0	18	12	0
2010 Oct	6	4	0	0	0

Notes. The number of integrations for each flux calibrator for nine 143 GHz Bolocam observing runs between 2003 and 2010. Note that there were five additional 143 GHz observing runs during that period, but those five observing runs included observations of only one flux calibration source and are therefore excluded from our analysis. Note that the typical S/N of each integration is >100.

Table 2
Bolocam 143 GHz Brightness Ratios

Date	$\frac{B_{\rm Uranus}}{B_{\rm Neptune}}$	$\frac{B_{\rm Uranus}}{B_{\rm NGC/G34}}$	$\frac{B_{\rm Neptune}}{B_{\rm NGC/G34}}$
2003 Nov	1.039 ± 0.045	1.029 ± 0.026	1.016 ± 0.042
2004 Nov	0.927 ± 0.065	...	...
2006 Nov	1.024 ± 0.010	1.006 ± 0.009	1.007 ± 0.010
2008 June	1.007 ± 0.022	1.010 ± 0.024	1.028 ± 0.015
2008 July	1.028 ± 0.017	1.038 ± 0.030	1.035 ± 0.032
2008 Nov	...	0.979 ± 0.012	...
2009 Oct	1.037 ± 0.011	0.995 ± 0.012	0.985 ± 0.008
2010 Feb	...	...	...
2010 Oct	1.054 ± 0.047	...	...
Total	1.027 ± 0.006	1.000 ± 0.006	1.000 ± 0.006

Notes. Brightness ratios of Uranus to Neptune, Uranus to the secondary calibrators NGC 2071IR and G34.3, and Neptune to the same secondary calibrators. Note that the brightness ratios of the planets to the secondary calibrators are normalized to the mean brightness ratio since the solid angle of the secondary calibrators is not precisely known. The brightness ratio of NGC 2071IR to G34.3 is constrained using the 2010 February data.

Fundamental to our flux calibration technique is the fact that Bolocam continuously monitors the operating resistance of the bolometers via the bias carrier amplitude. As the transmission of the atmosphere increases the optical load on the bolometers decreases and the operating resistance increases. Additionally, the responsivity (in nV $\rm Jy^{-1}$) of the bolometers increases as the bolometer resistance increases. Consequently, we are able to simultaneously account for changes in atmospheric transmission and detector responsivity by fitting the flux calibration as a function of bias carrier amplitude. In practice, the technique works as follows. For a given observing run, we generally observe multiple sources that have constant brightnesses. We then simultaneously fit the data for all of these sources according to

$$V_i(R_j) = B_i \Omega_{i,j} (\alpha_1 + \alpha_2 R_j),$$

where V_i is the bolometer response to source i (in nV), B_i is the brightness of source i, $\Omega_{i,j}$ is the solid angle of source i during observation j, R_j is the bolometer resistance during observation j as measured by the bias carrier amplitude, and α_1 and α_2 describe how the bolometer response changes as a function of R_j.

Implicit in the above formula is the assumption that changes in the overall opacity of the atmosphere are completely accounted for via α_1 and α_2, which implies that the atmospheric transmission varies in a such way that the shape of the Bolocam bandpass through the atmosphere is constant. However, over the range of conditions where these data were collected (column depths of precipitable water between 0.5 and 3.0 mm), variations in the atmospheric opacity do cause the Bolocam bandpass to vary slightly (Pardo et al. 2001a, 2001b, 2005). For a typical observing run, these bandpass variations in the atmosphere add an additional uncertainty of $\simeq$0.2% to our measured brightness ratios, which is negligible compared to our measurement uncertainties of 1%–5%.

Note that we have assumed that the angular size of the source is much smaller than the angular size of the Bolocam point-spread function (PSF), which is true for all of the sources.[1] Since the solid angle of both Uranus and Neptune varies with observation epoch, we compute the value of $\Omega_{i,j}$ separately for each integration of these planets using the James Clerk Maxwell Telescope (JCMT) Fluxes program.[2] For the secondary calibrators, the value of $\Omega_{i,j}$ is assumed to be constant. See Table 2 and Figure 1.

[1] The semi-diameters of the sources in arcsec are $\simeq$2 (Uranus), $\simeq$1 (Neptune), $\simeq$6 (NGC 2071IR), $\simeq$3.5 (G34.3), and $\simeq$4 (K3-50A), all of which are small compared to Bolocam's 59 arcsec full width at half-maximum point-spread function (Sandell 1994). The secondary calibrators are large enough that our point-like assumption will cause us to underestimate the total surface brightness of these objects by $\lesssim$1% (see Section 3). Uranus and Neptune are small enough that the correction is negligible (<0.1%).

[2] http://www.jach.hawaii.edu/jac-bin/planetflux.pl

3. RESULTS

Seven Bolocam observing runs contain observations of both Uranus and Neptune. In each run, we measure the brightness ratio of Uranus to Neptune with $\lesssim$5% statistical uncertainty. If we assume that the brightness ratio is constant over the period from 2003 to 2010, then we find that $B_{\rm Uranus}/B_{\rm Neptune} = 1.027 \pm 0.006$ with $\chi^2/{\rm DOF} = 4.5/6$. A linear fit versus year to the data reduces the value of χ^2 by 0.9, indicating that a linear fit is not required (an F-test shows that 39% of realizations of constant data would have yielded a larger F-ratio, implying that a constant fit to our data is adequate). Comparing to published results at similar frequencies, O86 find a brightness ratio of 1.016 ± 0.038 using 150 GHz data collected between 1983 February and 1984 March at the National Radio Astronomy Observatory 12 m antenna at Kitt Peak, and G93 find a brightness ratio of 1.043 ± 0.016 using 156 GHz data collected at the JCMT in 1990/1992 May. The combined $\simeq$150 GHz data set of O86, G93, and Bolocam is well described by a constant brightness ratio of $B_{\rm Uranus}/B_{\rm Neptune} = 1.029 \pm 0.006$, with a $\chi^2/{\rm DOF} = 5.4/8$. In this case a linear fit versus year reduces the value of χ^2 by 0.1, and an F-test shows that 76% of realizations of constant data would have produced a larger F-ratio. In addition, the linear fit provides a formal 95% confidence level upper limit of 5.3% on the magnitude of the variation over the 28 year period 1983–2010 (SEP latitudes of -82 to +10).

In addition to searching for variations in the brightness ratio of Uranus and Neptune, we also searched for temporal variations in the brightness of each planet relative to sources that are known to have constant brightnesses, NGC 2071IR and G34.3 (Sandell 1994). Six observing runs contained observations of Uranus and either NGC 2071IR or G34.3, and five observing runs contained observations of Neptune and either NGC 2071IR or G34.3. Note that we constrained the brightness ratio of NGC 2071IR and G34.3 based on observations of both objects in 2010 February. A constant fit of the brightness ratios yields a $\chi^2/{\rm DOF} = 6.3/5$ for Uranus and a $\chi^2/{\rm DOF} = 9.1/4$ for Neptune. We again calculate the F-ratio for a constant fit to the brightness ratios compared to a linear fit versus year and again find that there is no compelling evidence for a linear fit (22% of realizations of constant data would have a larger F-ratio than the Uranus data and 21% of realizations of constant data would have a larger F-ratio than Neptune data).

Since we are unable to measure any temporal variations in the brightnesses of Uranus or Neptune, we use the *WMAP* measurements of the brightness temperature of each planet (Weiland et al. 2011), along with our measurement of the brightness ratio (1.027), to determine the 143 GHz brightness temperature of each planet. In G93 the authors present models for the temperature spectra of each planet based on observations between 90 and 850 GHz, and we have used these models to extrapolate the 94 GHz *WMAP* measurements to 143 GHz. G93 state that these models are accurate to $<$2 K when absolute calibration uncertainties are not included, and we have therefore included a 2 K uncertainty in the model-based extrapolation of the absolute 94 GHz *WMAP* measurement to 143 GHz. We find that the brightness temperature of Uranus is 106.6 ± 3.5 K and the brightness temperature of Neptune is 103.8 ± 3.4 K, where the uncertainties include the *WMAP* and Bolocam measurement uncertainties, along with the quoted uncertainties in the G93 models. These brightness temperatures indicate that the G93 models need to be scaled by 0.931 ± 0.031 (Uranus) and 0.946 ± 0.031 (Neptune). Since the G93 brightness models of Uranus and Neptune were normalized to the Martian calibration model described in Griffin et al. (1986) (based on results from Wright 1976 and Ulich 1981), our results indicate that the Griffin et al. (1986) model overpredicts the brightness of Mars by $\simeq$5%–7%. These scalings are consistent with the results of Halverson et al. (2009), who find that the Wright (1976) model should be scaled by a factor of 0.922 ± 0.037 based on the *WMAP* Martian brightness measurements given in Hill et al. (2009).

Table 3
Absolute 143 GHz Brightness Values

Object	Brightness
Uranus	106.6 ± 3.5 K
Neptune	103.8 ± 3.4 K
NGC 2071IR	1.315 ± 0.043 Jy
G34.3	13.87 ± 0.47 Jy
K3-50A	7.387 ± 0.244 Jy

Notes. Absolute 143 GHz brightness values for calibrators observed by Bolocam. Uranus and Neptune are given in surface brightness units (K) and the secondary calibrators are given in units of peak flux density per beam (Jy).

Using these absolute brightness temperatures of Uranus and Neptune, we find peak flux densities per beam of $1.315 \pm 0.006 \pm 0.043$ Jy (NGC 2071IR), $13.87 \pm 0.10 \pm 0.46$ Jy (G34.3), and $7.387 \pm 0.009 \pm 0.244$ Jy (K3-50A) for the three secondary calibrators (see Table 3). The first value represents our measurement uncertainty on each peak flux density, while the second value represents our 3.3% uncertainty in the brightness temperatures of the planets. Given the source sizes in Sandell (1994), along with Bolocam's 59 arcsec FWHM PSF, these values should be within 1% of the total flux density for each source. Note that Sandell (1994) found the following peak flux densities per 27 arcsec beam for these sources at 150 GHz: 1.5 ± 0.2 Jy (NGC 2071IR), 12.5 ± 0.4 Jy (G34.3), and 6.5 ± 0.2 Jy (K3-50A), where the uncertainties do not include systematic uncertainties in the planet models used to calibrate the data. Our measured peak flux densities are $\simeq$10% higher for both G34.3 and K3-50A (plus an additional factor of $\simeq$7% due to the fact that Sandell 1994 used the G93 model in order to determine his absolute calibration, which we have found to overestimate the brightness of Uranus by $\simeq$7%). It is not clear why our measured peak flux densities are higher for G34.3 and K3-50A, although the known extended emission in both sources, coupled with the fact that Sandell (1994) made single-pixel chopped photometry measurements at 27 arcsec resolution, may be the cause.

4. DISCUSSION

We find that Uranus and Neptune behave as ideal sources for flux calibration at 143 GHz, with no evidence for temporal brightness variations. For Uranus, these results are in contrast to the lower frequency measurements of Kl06 and Kr08, who find $\simeq$0.5% yr^{-1} variations in the brightness temperature of Uranus at 8.6 and 90 GHz. Our data, combined with the measurements of O86 and G93, place a 95% confidence level upper limit of 0.19% yr^{-1} on the magnitude of variations in the brightness temperature of Uranus at $\simeq$150 GHz over the same period; see Figure 2. A physical interpretation of the temporal variations in the brightness of Uranus seen at lower frequencies by Kl06 and Kr08, in combination with our static 143 GHz results, is

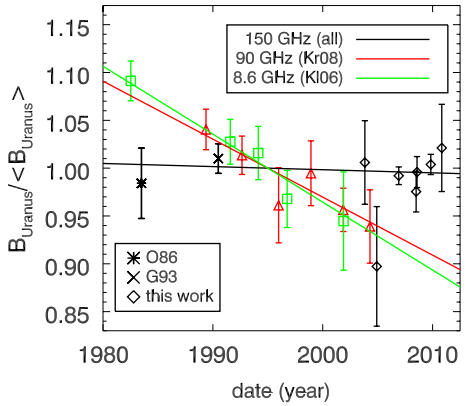

Figure 2. Uranus brightness measurements relative to the average brightness of Uranus at a range of frequencies between 1980 and 2010. The black points show ≃150 GHz data from O86, G93, and Bolocam, the red triangles show 90 GHz data from Kr08, and the green squares show 8.6 GHz data from Kl06 (taken from Table 2 of each paper and rebinned for visualization).

(A color version of this figure is available in the online journal.)

beyond the scope of this paper, which is intended to quantify the magnitude and stability of the brightness of Uranus for the purposes of using it as a calibrator at 143 GHz. However, we do note that the combined results are not necessarily inconsistent, given that higher frequency observations of Uranus probe higher altitudes in the atmosphere (Kr08).

5. CONCLUSIONS

Using Bolocam data collected between 2003 and 2010 we have tightly constrained the 143 GHz brightness ratio of Uranus and Neptune (1.027 ± 0.006), and we find no evidence for temporal variations in the 143 GHz brightness temperature of either planet over that period. Combining our results with those of O86 and G93, we find no evidence for 143 GHz brightness variations in either planet over the period from 1983 to 2010, and place a 95% confidence level upper limit of 5.3% on the magnitude of brightness variations over the 28 year period from 1983 to 2010. By extrapolating the *WMAP* 94 GHz results given in Weiland et al. (2011) to our observing band using the brightness models presented in G93, we are able to constrain the absolute 143 GHz brightness temperature of each planet to ≃3%. Additionally, we determine ≃3% absolute 143 GHz peak flux densities for the ultracompact H II regions G34.3 and K3-50A and the protostellar source NGC 2071IR.

We acknowledge the assistance of the Bolocam instrument team: Peter Ade, James Aguirre, James Bock, Sam Edgington, Jason Glenn, Alexy Goldin, Sunil Golwala, Douglas Haig, Andrew Lange, Glenn Laurent, Phil Mauskopf, Hien Nguyen, Philippe Rossinot, and Jack Sayers; Matt Ferry, Matt Hollister, Patrick Koch, Kai-Yang Lin, Sandor Molnar, Seth Siegel, and Keiichi Umetsu who, in addition to the Bolocam instrument team, helped collect the data presented in this manuscript; the day crew and Hilo staff of the Caltech Submillimeter Observatory, who provided invaluable assistance during commissioning and data-taking for this data set; Kathy Deniston, Barbara Wertz, and Diana Bisel, who provided effective administrative support at Caltech and in Hilo; and the referee, who provided helpful comments and suggestions. Bolocam was constructed and commissioned using funds from NSF/AST-9618798, NSF/AST-0098737, NSF/AST-9980846, NSF/AST-0229008, and NSF/AST-0206158. J.S. was partially supported by a NASA Graduate Student Research Fellowship, a NASA Postdoctoral Program Fellowship, NSF/AST-0838261, and NASA/NNX11AB07G; N.C. was partially supported by NASA Graduate Student Research Fellowship; S.G. acknowledges an Alfred P. Sloan Foundation Fellowship.

REFERENCES

Carlstrom, J. E., Ade, P. A. R., Aird, K. A., et al. 2011, PASP, 123, 903
Dowell, C. D., Allen, C. A., Babu, R. S., et al. 2003, Proc. SPIE, 4855, 73
Duncan, W. D., Robson, E. I., Ade, P. A. R., Griffin, M. J., & Sandell, G. 1990, MNRAS, 243, 126
Griffin, M. J., Ade, P. A. R., Orton, G. S., et al. 1986, Icarus, 65, 244
Griffin, M. J., & Orton, G. S. 1993, Icarus, 105, 537
Haig, D. J., Ade, P. A. R., Aguirre, J. E., et al. 2004, Proc. SPIE, 5498, 78
Halverson, N. W., Lanting, T., Ade, P. A. R., et al. 2009, ApJ, 701, 42
Hill, R. S., Weiland, J. L., Odegard, N., et al. 2009, ApJS, 180, 246
Holland, W. S., MacIntosh, M., Fairley, A., et al. 2006, Proc. SPIE, 6275, 62751E
Holland, W. S., Robson, E. I., Gear, W. K., et al. 1999, MNRAS, 303, 659
Klein, M. J., & Hofstadter, M. D. 2006, Icarus, 184, 170
Kramer, C., Moreno, R., & Greve, A. 2008, A&A, 482, 359
Laurent, G. T., Aguirre, J. E., Glenn, J., et al. 2005, ApJ, 623, 742
Orton, G. S., Griffin, M. J., Ade, P. A. R., Nolt, I. G., & Radostitz, J. V. 1986, Icarus, 67, 289
Orton, G., Hotstadter, H., Leyrat, C., & Encrenaz, T. 2007, in Workshop on Planetary Atmospheres, 2007 November 6–7, Greenbelt, Maryland (LPI Contribution 1376) (Houston, TX: Lunar and Planetary Institute), 93
Page, L., Jackson, C., Barnes, C., et al. 2003, ApJ, 585, 566
Pardo, J. R., Cernicharo, J., & Serabyn, E. 2001a, IEEE Trans. Antennas Propag., 49, 1683
Pardo, J. R., Serabyn, E., & Cernicharo, J. 2001b, J. Quant. Spectrosc. Radiat. Transfer, 68, 419
Pardo, J. R., Serabyn, E., Wiedner, M. C., & Cernicharo, J. 2005, J. Quant. Spectrosc. Radiat. Transfer, 96, 537
Reichardt, C. L., Ade, P. A. R., Bock, J. J., et al. 2009, ApJ, 694, 1200
Rudy, D. J., Muhleman, D. O., Berge, G. L., Jokosky, B. M., & Christensen, P. R. 1987, Icarus, 71, 159
Runyan, M. C., Ade, P. A. R., Bhatia, R. S., et al. 2003, ApJS, 149, 265
Sandell, G. 1994, MNRAS, 271, 75
Sayers, J., Golwala, S. R., Rossinot, P., et al. 2009, ApJ, 690, 1597
Swetz, D. S., et al. 2011, ApJS, 194, 41
Ulich, B. L. 1981, AJ, 86, 1619
Weiland, J. L., Odegard, N., Hill, R. S., et al. 2011, ApJS, 192, 19
Wright, E. L. 1976, ApJ, 210, 250